Journal of Computational Information Systems 8: 10 (2012) 4031–4038
Available at http://www.Jofcis.com

Evaluation of the Projection Ordering for Cone-beam CT ⋆

Huihua KONG, Jinxiao PAN*

School of Science, North University of China, Taiyuan 030051, China

Abstract

The major disadvantage of the iterative algorithms for cone-beam x-ray CT such as algebraic reconstruction techniques (ART) is the slow convergence due to the large data sets and the high number of iterations required for reconstructing high resolution images. The convergence speed of ART heavily depends on the order in which the projections are accessed. The methods for choosing the order of the projections for parallel and fan beams have been proposed in previous studies. In this paper, we analyse quantitatively the correlation of two rays in different views and the use of projection ordering for cone-beam x-ray CT reconstruction, for the case of circular acquisition orbits. We focus on the reconstructed image accuracy of the 3D Shepp-Logan model. Experiments show that when the angle interval of projection is less than 6°, reasonable adjustment of the projection views can accelerate the speed of the reconstruction and improve the quality of the reconstruction. However, when the angle interval of projection is beyond 6°, changing the projection ordering has little effect on the convergence of ART.

Keywords: Iterative Algorithm; Cone-beam CT; Projection Ordering; Convergence Speed

1 Introduction

Cone-beam x-ray computed tomography (CT) has two major categories of image reconstruction: analytic methods and iterative methods. Iterative methods for image reconstruction such as algebraic reconstruction techniques (ART) [1]are more robust and flexible than analytical inversion methods in handling incomplete, noisy, and dynamic data. The ART is a tomographic reconstruction method that reconstructs a three-dimensional (3D) object from its projection images which are acquired from any projective imaging modality, such as x-ray, positron emission tomography (PET) or single photon emission computed tomography (SPECT). This method was originally proposed by Kaczmarz in 1937 [2] and was first published for CT by Gordon etc. in 1970 [1].

Let $Y = (y_i) \in \mathbb{R}^I$ is the projection data, $X = (x_j) \in \mathbb{R}^J$is the image vector and $A = (a_{ij})_{I\times J}$ is the projection matrix, a_{ij} is the length of the intersection of the j-th voxel with projection

⋆Project supported by the National Natural Science Foundation of China (No. 61171179, 61071193) and the Natural Science Foundation of Shanxi province (2010011002-1)

*Corresponding author.
Email address: `fengerkong@nuc.edu.cn` (Jinxiao PAN).

May 15, 2012

ray i. There are several different choices of a_{ij} in other research [3-5]. The image reconstruction problem in CT can be modeled by the following equation:

$$AX = Y. \tag{1}$$

The problem is to reconstruct X from Y. A direct solution might be infeasible, because of the ill-conditioning problem. The ART provides an efficient iterative way to solve the linear system of equations (1). It can be written as:

$$x_j^{(k+1)} = x_j^{(k)} + \lambda_k \cdot \frac{y_i - \sum\limits_{j=1}^{J} a_{ij} x_j^{(k)}}{\sum\limits_{j=1}^{J} a_{ij}^2} \cdot a_{ij}, \tag{2}$$

where $i = (k \bmod I) + 1$ and λ_k is the relaxation parameter. ART applies only one ray to update the entire image at each step. It was shown by Andersen and Kak [6] that noise-like artifacts in the reconstruction can be reduced if the voxel is corrected only once per projection image and not for every projection ray. This discovery gave rise to SART:

$$x_j^{(k+1)} = x_j^{(k)} + \lambda_k \cdot \frac{1}{\sum\limits_{i \in P_l} a_{ij}} \sum_{i \in P_l} \frac{y_i - \sum\limits_{j=1}^{J} a_{ij} x_j^{(k)}}{\sum\limits_{j=1}^{J} a_{ij}} \cdot a_{ij}, \tag{3}$$

where P_l is the projection image at $(l+1)$-th view.

The rate of convergence of the iterative reconstruction depends on the order in which the collected data are accessed during the reconstruction procedure. Several observations have been made on the improvements of the projection access systems for parallel beam and fan beam [7-11]. However even now, there is no gold standard in this branch of tomography. Generally speaking, Random Access Scheme (RAS) [7], Prime Number Decomposition (PND) principle [8], Multilevel Access Scheme (MLS) [9], Weighted Distance Scheme (WDS) [10] and Golden ratio-based (GR) ordering [11] are considered effective orderings.

The aim of this paper is to tackle the problem of optimal ordering of projections processed by iterative procedures, for cone-beam x-ray CT reconstruction, for the case of circular acquisition orbits. The structure of this paper is as follows. In section 2, we analyse the correlation between two rays in different views. The four different projection ordering systems are introduced in section 3. Section 4 describes the experiments, quantitative evaluation metrics and the results. The conclusion is given in section 5.

2 The Correlation Between the Two Rays

Let A_i be the i-th row of the projection matrix A, then $A_i = (a_{i1}, a_{i2}, \cdots, a_{iJ}), i = 1, 2, \cdots, I$. In the N-dimension space, the cosine of the hyperangle formed by two hyperplanes A_j and A_k is defined as

$$\cos \alpha_{j,k} = \frac{A_j \cdot A_k}{|A_j| \cdot |A_k|}. \tag{4}$$

In general, $|\cos\alpha_{j,k}| \leqslant 1, \cos\alpha_{j,k} = 0$ means that the two hyperplanes are orthogonal to each other; the higher the $|\cos\alpha_{j,k}|$ is, the stronger the correlation between the two hyperplanes is. Guan and Gordon analysed the correlation of two rays in one view and concluded that reordering the rays in each view would have little effect on the convergence performance for parallel beam and divergent beam.

In the following, we focus on the correlation between the two rays that are not in the same view for cone-beam scanning mode, for the case of circular acquisition orbits. Fig. 1 gives the geometry diagram of cone beam scanning system based on the plat panel detector and Fig. 2 gives the sketch of flat panel detector. Set the origin of the coordinate system is located at the center of the object, then the projection of the coordinate' origin in the flat panel detector is located in the central position of detector.

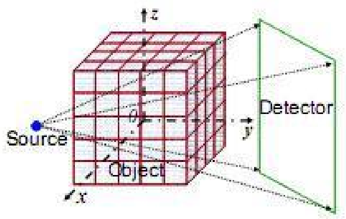

Fig. 1: The geometry diagram of cone beam scanning system

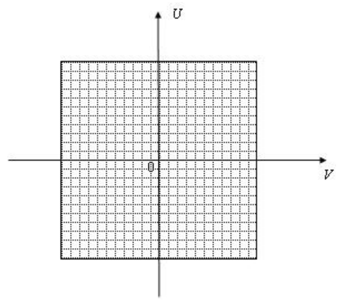

Fig. 2: The sketch of flat panel detector

Using formula (4) calculates the correlation between the two rays in different views. Assuming the test model is $128 \times 128 \times 128$ voxels; the detector plane contains 160×160 detection channels; the distance from source to detector plane equals to 1300 pixels and the distance from source to centre of rotation equals to 1000 pixels. Fig. 3 gives the correlation between the ray at the center of the detector plane in the view of $0°$ and the ray in other views. The interval of any two rays is 0, 1, 2 pixel, respectively. We can see from Fig. 3 that the correlation of the two rays decrease gradually with the increasing the angle interval between the two views. When the angle interval is beyond $6°$, the cosine of the hyperangle defined as equation (4) is almost less than $0.2(\alpha_{j,k} \approx 78°)$, so we can think the two rays between the different views is not related and it is not necessary to reordering the projection views.

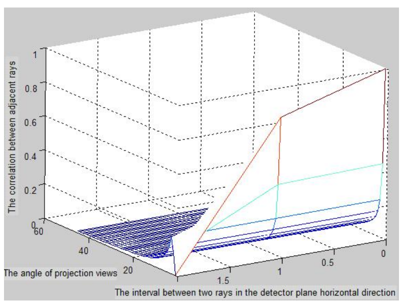

Fig. 3: The correlation between the ray at the center of the detector plane in the view of $0°$ and the ray in other views. The interval of any two rays is 0, 1, 2 pixel, respectively

3 Projection Ordering Systems

Considering that the projection views generated from GR are non-uniform, in the experiments, we compare the sequential access (SAS), random access system (RAS), PND, MLS and WDS. We now introduce the projection ordering systems RAS, PND, MLS and WDS. Let P is the total number of views to be ordered.

In 1992, Van Dijke proposed RAS and concluded that using the projection randomly, rather than in the given order, can greatly improve the rate of convergence of iterative algorithms [7].

In 1993, Herman and Meyer designed a permutation operation based on the Prime Number Decomposition (PND) principle. This method demands the P is non prime and can be decomposed into prime factors

$$P = P_U \times \cdots \times P_2 \times P_1 (P_U \geqslant \cdots \geqslant P_2 \geqslant P_1). \tag{5}$$

Let T be the set of U-dimensional vectors t, whose u-th component t_u is an integer which satisfied:

$$0 \leqslant t_u \leqslant P_u - 1 (1 \leqslant u \leqslant U). \tag{6}$$

The permutation π is a one-to-one mapping of $T = (t_1, t_2, \cdots, t_U)$ onto the range $[0, P)$ of integers, the algorithm is as following:

```
k = 0
for t_U = 0 : P_U − 1
  ......
  for t_2 = 0 : P_2 − 1
    for t_1 = 0 : P_1 − 1
      T(k) = (t_1, t_2, ··· , t_U)
      π(k) = (P_U × P_{U−1} × ··· × P_2 × t_1) + (P_U × P_{U−1} × ··· × P_3 × t_2) + ··· + (P_U × t_{U−1}) + t_U
      k = k + 1
    end
  end
end
```

In 1994, Guan and Gordon, who considered the effect of geometrical correlation of projections, presented the Multilevel Access Scheme (MLS), which works best when the number of projections is a power of 2.

When a given number of projections is not a power of two, it can also be used with minor modifications. The total levels is $L = [\log_2 P] + 1$ ([ ]=truncate to integer). From level $l = 1$ to $L - 1$, the implementation of the ordering is exactly the same as that for the case with P a power of two but just rounding the values to integers. In the level L, only the $P - 2^{L-1}$ views are taken. Additional work needs to be done since occasionally the calculated value may have been already accessed. If so, we search both sides of the value until the closest unused value is found and then put it into the sequence and set a flag. In general it is just the neighbour or next neighbour.

In 1997, Klaus Mueller proposed a globally optimizing projection access algorithm, the Weighted Distance Scheme (WDS) [10], which optimizes the selection in a global sense and considers the projection selection at iteration boundaries. In the WDS, a new view is chosen that has the maximum distance from the previously chosen views, as shown in Fig. 5. The greater distance between the views indicates that the views can cover the wider field-of-view to be reconstructed. Detailed steps are as follows:

Step 1: Compute weighted mean of the 'repulsive forces': $\mu_l = \frac{\sum_{q=0}^{Q-1} w_q(S/2-d_{lq})}{\sum_{q=0}^{Q-1} w_q}$, projection distance:$d_{lq} = \min(|l-q|, S-|l-q|)$, weight: $w_q = (q+1)/Q$;

Step 2: Weight standard deviation of projection distance d_{lq}: $\sigma_l = \left[\frac{\sum_{q=0}^{Q-1} w_q(d_{lq}-\bar{d}_l)^2}{\sum_{q=0}^{Q-1} w_q}\right]^{\frac{1}{2}}$,$\bar{d}_l = \frac{\sum_{q=0}^{Q-1} w_q d_{lq}}{Q}$;

Step 3: Standardization $\tilde{\mu}_l = \frac{\mu_l - \min_{k\in\wedge}(\mu_k)}{\max_{k\in\wedge}(\mu_k) - \min_{k\in\wedge}(\mu_k)}$, $\tilde{\sigma}_l = \frac{\sigma_l - \min_{k\in\wedge}(\sigma_k)}{\max_{k\in\wedge}(\sigma_k) - \min_{k\in\wedge}(\sigma_k)}$;

Step 4: Select elements from the set $\wedge$, so to meet the $\min_{l\in\wedge}(D_l), D_l = \tilde{\mu}_l^2 + 0.5 \cdot \tilde{\sigma}_l^2$.

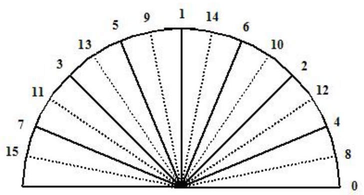

Fig. 4: The projection orders for sixteen projections in the MLS

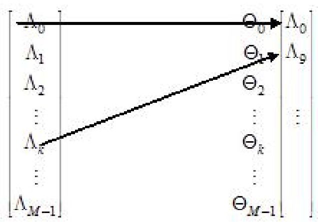

Fig. 5: Projection selection process in WDS

The goal of this paper is to analyse the use of different projection ordering for cone-beam x-ray CT reconstruction, for the case of circular acquisition orbits.

4 Experiments

The 3D $128 \times 128 \times 128$ voxels Shepp-Logan model is selected as the test model and two sets of experiments are conducted to implement the comparative studies. In the comparative studies, the reconstruction algorithm is SART and projection ordering involves SAS, RAS, PND, MLS and WDS.

We use a circular orbit to acquire the projection views which are distributed uniformly in angle $[0, \pi)$ and the angle interval between the two projections is $1°$, $6°$ respectively. The detector plane contains 160×160 detection channels. The distance from source to detector plane equals to 1300 pixels and the distance from source to centre of rotation equals to 1000 pixels. To eliminate the effects of another variable in the comparative process, we used a fixed value of $\lambda_k = 0.3$ throughout the reconstruction procedure.

The normalized mean square error (NRMSE) is defined as:

$$\mathrm{NRMSE} = \left[\frac{\sum_{i=1}^{J} (x_i - \widehat{x}_i)^2}{\sum_{i=1}^{J} (x_i - \overline{x})^2} \right]^{\frac{1}{2}}, \tag{7}$$

where x_i refers to the i-th voxel value in the true image, $\widehat{x}_i$ represents the value of voxel i in the reconstructed image and $\overline{x}$ represents the image average value in the true image. This measure quantifies the overall difference between the reconstructed image and the true image, and can be used to evaluate the convergence rate of the algorithm.

The correlation coefficient (CC) is defined as

$$\mathrm{CC} = \frac{\sum_{i=1}^{J} (x_i - \overline{x})(\widehat{x}_i - \tilde{x})}{\left[\sum_{i=1}^{J} (x_i - \overline{x})^2 \cdot \sum_{i=1}^{J} (\widehat{x}_i - \tilde{x})^2 \right]^{\frac{1}{2}}}, \tag{8}$$

where $\tilde{x}$ represent image average value in the reconstructed images. The CC measures the extent to which two images are similar to each other and it takes the highest value of unity if the two are exactly the same.

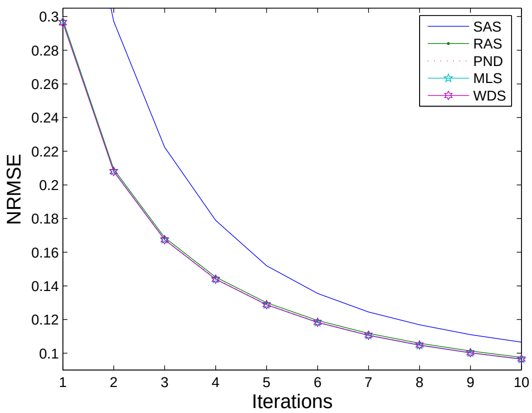

(a) The angle interval of projection sampling is 1°

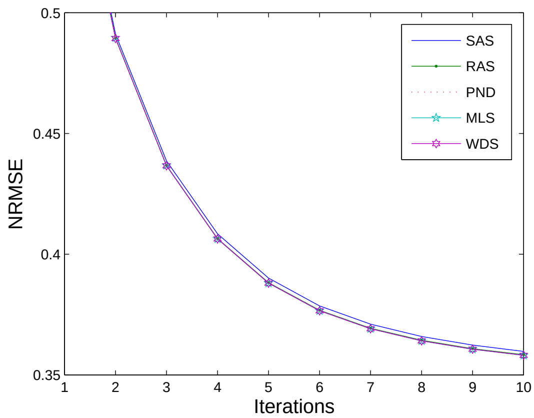

(b) The angle interval of projection sampling is 6°

Fig. 6: The NRMSE as a function of iterations for five different projection ordering systems

Fig. 6 gives the plots of the NRMSE as a function of the iteration number using different projection orders for two angle interval. We can see obviously from Fig. 6 that SAS yields larger NRMSE than other four orders when the angle interval of projection is 1°. This implies that reasonable adjustment of the projection views can accelerate the speed of the reconstruction and improve the quality of the reconstruction. However, with increasing the angle interval of projection, the difference of convergence for the different projection orderings is gradually decreasing. When the angle interval is beyond 6°, changing the projection ordering has little effect on the convergence of SART. This phenomenon is consistent with the analysis in the section 2. Because the difference among the RAS, PND, MLS and WDS is very small, we almost see no difference from Fig. 6. To compare the quality of the reconstructions further, Table 1 lists the CC versus iterations when the angle interval is 1°. From table 1, we note that the maximum error at the same number of iterations is less than 7.95×10^{-4}.

Table 1: The CC versus iterations when the angle interval is 1°

Iterations	SAS	RAS	PND	MLS	WDS
1	0.911861	0.952788	0.953422	0.953463	0.953583
2	0.951040	0.974741	0.974921	0.975023	0.975103
3	0.968353	0.981975	0.982097	0.982197	0.982234
4	0.977510	0.985511	0.985624	0.985680	0.985705
5	0.982896	0.987707	0.987807	0.987859	0.987890
6	0.985427	0.989146	0.989259	0.989284	0.989291
7	0.987840	0.990076	0.990174	0.990216	0.990205
8	0.988775	0.990815	0.990943	0.990969	0.990965
9	0.990121	0.991453	0.991544	0.991570	0.991551
10	0.990729	0.991912	0.991998	0.992017	0.991995

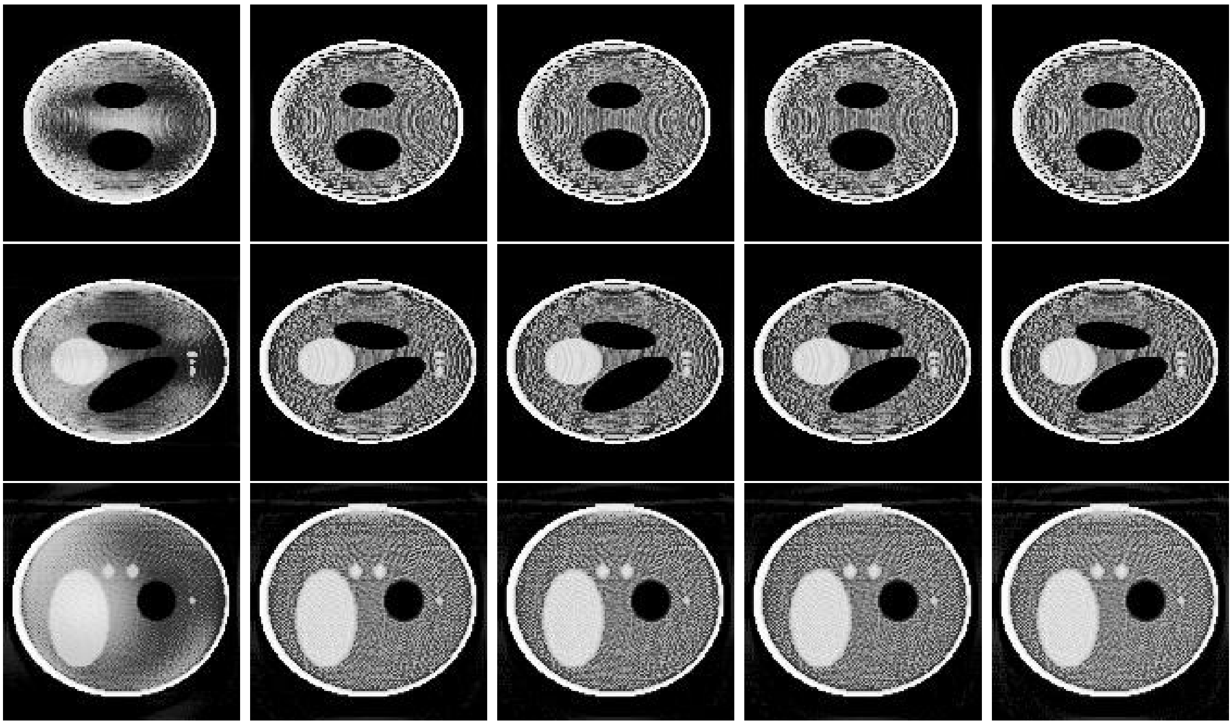

(a) SAS (b) RAS (c) PND (d) MLS (e) WDS

Fig. 7: Reconstruction results at the central location of three different axes after three iterations

The three central slices of the reconstruction after three iterations using the five projection ordering schemes are shown in Fig. 7 for the first set of projection data. The graph clearly shows the quality of the image reconstructed by SAS be worse than that reconstructed by RAS, PND, MLS and WDS, since there are some visible low-frequency artifacts in Fig. 7(a). While the other four orders reconstruction images have little difference shown as Fig. 7(b,c,d,e).

5 Conclusion

In this study, we have analysed the impact of different projection orders on the convergence of iterative algorithms. Quantitative error measurements show that when the angle interval of projection is less than 6°, reasonable adjustment of the projection views can accelerate the speed of the reconstruction and improve the quality of the reconstruction and when the angle interval of projection is beyond 6°, changing the projection ordering has little effect on the convergence of SART. We also see from the experiments that there are no significant difference between the RAS, PND, MLS and WDS.

References

[1] R. Gordon, R. B. ender, G. T. Herman. Algebraic reconstruction techniques (ART) for three-dimensional electron microscopy and X-ray photography. J. Theoret. Biol., 29 (1970), 471 – 481.

[2] S. Kaczmarz. Angenäherte Auflösung von Systemen linearer Gleichungen. Bull. Acad. Polon. Sci. Lett. A, (1937) 335 – 357.

[3] R. Gordon, A tutorial on ART. IEEE Transactions on Nuclear Science, 21 (1974), 78 – 93.

[4] K. Mueller. Fast and accurate three-dimensional reconstruction from cone-beam projection data using Algebraic methods, Ph. D. dissertation, The Ohio State University, Columbus, 1998.

[5] Yue Zhao, XiaoHua Hu, Yue Chen. Parallel planes and infinite points based three-dimensional reconstruction. Journal of Computational Information Systems, 6 (2010), 3559 – 3566.

[6] A. H. Andersen, A. C. Kak. Simultaneous algebraic reconstruction technique (SART): A superior implementation of the ART algorithm. Utrason. Imag., 6 (1984), 81 – 94.

[7] M. C. van Dijke. Iterative methods in image reconstruction. Ph. D. Dissertation, Rijksuniversiteit Utrecht, The Netherlands, 1992.

[8] G. T. Herman and L. B. Meyer. Algebraic reconstruction technique can be made computationally efficient. IEEE Trans. Med. Imag., 12 (1993), 600 – 609.

[9] H. Guan and R. Gordon. A projection access order for speedy convergence of ART (algebraic reconstruction technique): a multilevel scheme for computed tomography. Phys. Med. Biol., 39 (1994), 2005 – 2022.

[10] K. Mueller, R. Yagel and F. Cornhill. The weighted distance scheme: A Globally Optimizing Projection Ordering Method for ART. IEEE Trans. Med. Imag. 16 (1997), 223 – 230.

[11] T. Köhler. A Projection Access Scheme for Iterative Reconstruction Based on the Golden Section. in: Proc. of the 2004 IEEE Nuclear Science and Medical Imaging Conference, CDROM M10-200, Rome, Italy, October 16 – 22, (2004), 3961 – 3965.